HHS Public Access

Author manuscript

*Bioorg Med Chem*. Author manuscript; available in PMC 2019 May 01.

Published in final edited form as:

*Bioorg Med Chem*. 2018 May 01; 26(8): 1939–1949. doi:10.1016/j.bmc.2018.02.040.

# Fluorine-18 labeling of an anti-HER2 VHH using a residualizing prosthetic group via a strain-promoted click reaction: chemistry and preliminary evaluation

**Zhengyuan Zhou**[a], **Satish K Chitneni**[a], **Nick Devoogdt**[b], **Michael R. Zalutsky**[a], and **Ganesan Vaidyanathan**[a,*]

[a]Department of Radiology, Duke University Medical Center, Durham, North Carolina, USA 27710

[b]In Vivo Cellular and Molecular Imaging Laboratory, Vrije Universiteit Brussel, (VUB), 1090, Brussels, Belgium

## Abstract

In a previous study, we evaluated a HER2-specific single domain antibody fragment (sdAb) 2Rs15d labeled with $^{18}$F via conjugation of a residualizing prosthetic agent that was synthesized by copper-catalyzed azide-alkyne cycloaddition (CuAAC). In order to potentially increase overall efficiency and decrease the time required for labeling, we now investigate the use of a strain-promoted azide-alkyne cycloaddition (SPAAC) between the 2Rs15d sdAb, which had been pre-derivatized with an azide-containing residualizing moiety, and an $^{18}$F-labeled aza-dibenzocyclooctyne derivative. The HER2-targeted sdAb 2Rs15d and a nonspecific sdAb R3B23 were pre-conjugated with a moiety containing both azide- and guanidine functionalities. The thus derivatized sdAbs were radiolabeled with $^{18}$F using an $^{18}$F-labeled aza-dibenzocyclooctyne derivative ([$^{18}$F]F-ADIBO) via SPAAC, generating the desired conjugate ([$^{18}$F]RL-II-sdAb). For comparison, unmodified 2Rs15d was labeled with *N*-succinimidyl 4-guanidinomethyl-3-[$^{125}$I]iodobenzoate ([$^{125}$I]SGMIB), the prototypical residualizing agent for radioiodination. Radiochemical purity (RCP), immunoreactive fraction (IRF), HER2-binding affinity and cellular uptake of [$^{18}$F]RL-II-2Rs15d were assessed in vitro. Paired label biodistribution of [$^{18}$F]RL-II-2Rs15d and [$^{125}$I]SGMIB-2Rs15d, and micro-PET/CT imaging of [$^{18}$F]RL-II-2Rs15d and the [$^{18}$F]RL-II-R3B23 control sdAb were performed in nude mice bearing HER2-expressing SKOV-3 xenografts. A radiochemical yield of 23.9 ± 6.9% (n=8) was achieved for the SPAAC reaction between [$^{18}$F]F-ADIBO and azide-modified 2Rs15d and the RCP of the labeled sdAb was >95%. The affinity ($K_d$) and IRF for the binding of [$^{18}$F]RL-II-2Rs15d to HER2 were 5.6 ± 1.2 nM and 73.1 ± 22.5 % (n=3), respectively. The specific uptake of [$^{18}$F]RL-II-2Rs15d by HER2-expressing BT474M1 breast carcinoma cells in vitro was 14–17% of the input dose at 1, 2, and 4 h, slightly higher than seen for co-incubated [$^{125}$I]SGMIB-2Rs15d. The uptake of [$^{18}$F]RL-II-2Rs15d in SKOV-3 xenografts at 1 h and 2 h p.i. were 5.54 ± 0.77% ID/g and 6.42 ± 1.70% ID/g,

*Corresponding Author: Ganesan Vaidyanathan, Ph.D., 161C, Bryan Research Building, 311 Research Drive, Durham, North Carolina 27710, USA. Tel.: (919) 684-7811; ganesan.v@duke.edu.

respectively, slightly higher than those for co-administered [$^{125}$I]SGMIB-2Rs15d (4.80 ± 0.78% ID/g and 4.78 ± 1.39% ID/g). Micro-PET/CT imaging with [$^{18}$F]RL-II-2Rs15d at 1–3 h p.i. clearly delineated SKOV-3 tumors while no significant accumulation of activity in tumor was seen for [$^{18}$F]RL-II-R3B23. With the exception of kidneys, normal tissue levels for [$^{18}$F]RL-II-2Rs15d were low and cleared rapidly. To our knowledge, this is the first time SPAAC method has been used to label an sdAb with $^{18}$F, especially with residualizing functionality.

## Graphical Abstract

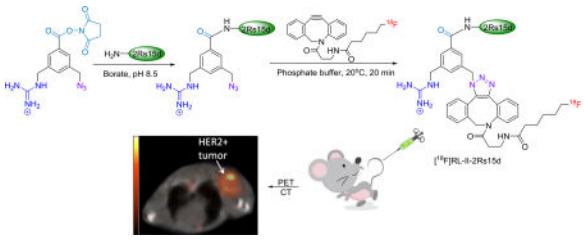


### Keywords

Fluorine-18; strain-promoted click reaction; VHH; HER2; residualizing label

## 1. Introduction

Single-domain antibody fragments (sdAbs), also known as nanobodies (Nbs) and VHH molecules, are derived from camelid heavy-chain-only antibodies. Compared with other protein-based vehicles, advantages of sdAbs include stability, low immunogenicity, and nanomolar to picomolar affinity. To date, a variety of sdAb-based agents specific to oncological targets such as epidermal growth factor receptor (EGFR) [1–3], prostate-specific membrane antigen (PSMA) [4–6], multiple myeloma 5T2 M-protein [7, 8], and human epidermal growth factor receptor type 2 (HER2) [9–11] have been developed and evaluated both preclinically and clinically. The small size (~15 kDa) of sdAbs facilitates vascular extravasation and tissue penetration as well as rapid blood clearance. The latter property makes them excellent vehicles for molecular imaging with short-lived positron emitters such as $^{18}$F and $^{68}$Ga.

HER2 overexpression occurs in about 20% of breast cancers and is generally associated with tumor aggressiveness [12]. Therefore, robust assessment of HER2 status is crucial for selecting patients who might benefit from HER2-targeted treatments. Current methods for the assessment of HER2 status – immunohistochemistry and fluorescence in situ hybridization – are not ideal because they require invasive biopsy and are inappropriate for dealing with the heterogeneous nature of HER2 expression in the primary tumor as well as variability in expression between primary and metastatic tumors [13]. Furthermore, these methods do not provide tumor HER2 status in real-time. Given the risks involved in invasive procedures and the potential for misleading results from these ex-vivo methods, non-invasive alternatives that can provide global HER2 status in real time are needed. Positron emission tomography (PET) is a molecular imaging technique with high quantitative capability, making PET an attractive approach for achieving this goal.

Certain biomolecules undergo internalization after binding to their respective receptors/antigens on the surface of tumor cells, translocate to the lysosomes wherein they are catabolized. When these molecules are radiolabeled, the low molecular weight catabolites bearing the radiolabel often wash out of the cells decreasing the radioactive signal within the tumor cells. Residualizing prosthetic agents, containing charged or polar moieties, carbohydrate residues, and/or D-amino acid peptides generate cell- and lysosome-membrane-impermeable catabolites, thereby increasing activity retention in the tumor cells after internalization [14, 15]. In a previous study, we labeled the anti-HER2 sdAb 2Rs15d with $^{18}$F using a residualizing label ([$^{18}$F]RL-I) designed to entrap the $^{18}$F in HER2-expressing cancer cells after receptor-mediated internalization. The [$^{18}$F]RL-I prosthetic group was pre-synthesized employing conventional Cu(I)-assisted [3+2] Huisgen alkyne-azide cycloaddition (CuAAC) [16]. The thus labeled 2Rs15d ([$^{18}$F]RL-I-2Rs15d) demonstrated good immunoreactivity and affinity for HER2 as well as specific tumor targeting in vivo. However, the labeling procedure required about 3 h and the overall radiochemical yield was only 3–4%. One approach for streamlining the labeling procedure and potentially increasing the radiochemical yield is the use of bioorthogonal chemistry to directly label the sdAb. Although attempts have been made to label proteins and other biomolecules using CuAAC [17–19], limitations of CuAAC include the toxicity of copper as well as its potential for forming complexes with biomolecules [20]. A copper-free, strain-promoted azide-alkyne cycloaddition (SPAAC) has been developed to surmount these problems [21] and SPAAC has been utilized successfully with both nonradiolabeled and radiolabeled prosthetic agents to modify peptides, which can tolerate relatively harsh conditions like higher temperature and organic solvents [20, 22]. Proteins also have been modified using SPAAC with nonradiolabeled prosthetic agents, where one has the luxury of using stoichiometric or excess amounts of the agent, and running the reaction for an extended period [23]. Of some relevance to this work, SPAAC has been used to generate dimeric sdAbs and to PEGylate an sdAb [24]. To our knowledge, SPAAC has not been utilized for labeling proteins with radionuclides, particularly those with short half-lives like $^{18}$F ($t_{1/2}$ = 109.8 min). It should be noted that during the final stages of preparing this manuscript, labeling of an Adnectin protein with $^{18}$F by a similar approach was published [25]; however, this method did not involve introduction of a residualizing label that was designed for use with an internalizing biomolecule like 2Rs15d anti-HER2 sdAb.

The aim of this study was to develop a method for labeling 2Rs15d with $^{18}$F using a residualizing label via SPAAC. This was accomplished by first pre-conjugating the sdAb with the azide- and guanidine-containing prosthetic moiety *N*-succinimidyl 3-(azidomethyl)-5-(guanidinomethyl)benzoate (**1**) [26] and then clicking the derivatized 2Rs15d with [$^{18}$F]F-ADIBO [27] (Scheme 1). This radiolabeled sdAb was evaluated on HER2-expressing cell lines and by necropsy biodistribution and microPET imaging in athymic mice bearing HER2-expressing SKOV-3 ovarian carcinoma xenografts. As a benchmark for comparison, 2Rs15d radiolabeled with the prototypical radioiodination residualizing label [$^{125}$I]SGMIB was evaluated in parallel.

## 2. Materials and Methods

### 2.1. General

All reagents were purchased from Sigma-Aldrich except where noted. Sodium [$^{125}$I]iodide (81.4 TBq (2200 Ci)/mmol) in 0.1 N NaOH was obtained from Perkin-Elmer Life and Analytical Sciences (Boston, MA). Synthesis of *N*-succinimidyl 4-guanidinomethyl-3-[$^{125}$I]iodobenzoate ([$^{125}$I]SGMIB) [14] and *N*-succinimidyl 3-(azidomethyl)-5-((1,2-bis(*tert*-butoxycarbonyl)guanidino)methyl)benzoate [26] has been described. The sdAb 2Rs15d was radioiodinated using [$^{125}$I]SGMIB as reported before [16]. *N*-(3-aminopropionyl)-5,6-dihydro-11,12-didehydrodibenzo[b,f]azocine (ADIBO-amine; compound **2**, Scheme 2) was obtained from Click Chemistry Tools (Scottsdale, AZ). Normal phase column chromatography was performed using the Biotage Isolera chromatography system (Charlotte, NC) and their prepacked columns. High performance liquid chromatography (HPLC) was performed using the following systems: 1) An Agilent 1260 MWD system with PrepStar 218 pumps and controlled by the Agilent ChemStation software (this system was used for purification of compound **1**) 2) an Agilent 1260 Infinity system equipped with a 1260 Infinity Multiple Wavelength Detector (Santa Clara, CA) connected to a LabLogic Dual Scan-RAM flow radioactivity detector/TLC scanner (Tampa, FL); the whole system was controlled by LabLogic Laura® software. In addition, for semi-preparative HPLC purification of compounds **5** and **6**, the Agilent HPLC attached to the LCMS (see below) was used. When the Agilent system was used, for both radiolabeled and unlabeled compounds, HPLC was performed using an Agilent Poroshell EC-120 (9.4 × 250 mm 2.7 μm) reversed-phase semi-preparative column. Empore™ SPE C18 cartridges used for concentrating HPLC samples were purchased from 3M (Maplewood, MN). Disposable PD 10 desalting columns for gel filtration were purchased from GE Healthcare (Piscataway, NJ). Instant thin layer chromatography (ITLC) was performed using silica gel impregnated glass fiber sheets (Pall Corporation, East Hills, NY) using PBS, pH 7.4 as the mobile phase. Developed sheets were analyzed for activity using the TLC scanner described above. Activity levels in various samples were assessed using either an LKB 1282 (Wallac, Finland) or Perkin Elmer Wizard II (Shelton, CT) automated gamma counter. Proton NMR spectra were obtained on a 400 MHz spectrometer (Varian/Agilent, Inova; Palo Alto, CA) and chemical shifts are reported in δ units using the residual solvent peaks as a reference. For compound **1**, both proton and $^{13}$C-NMR spectra were obtained using a Varian 500 MHz (125.8 MHz) spectrometer. Mass spectra were recorded using an Agilent LC/MSD Trap for electrospray ionization (ESI) LC/MS and/or an Agilent LCMS-TOF (ESI); the latter is a high-resolution mass spectrometer. In addition, mass spectra were also obtained using an Advion (Ithaca, NY) Expression$^{L}$ CMS LC-MS System attached to an Agilent HPLC like the one described above. This equipment has the capability of determining molecular weights of compounds directly from TLC plates (Plate Express) and by ESI, APCI, and ASAP. For the determination of derivatized sdAb molecular weights, either the above Advion system (LCMS) or an Applied Biosystems DE-PRO Biospectrometry Workstation (for Maldi) were used. Surface plasmon resonance experiments were performed on a GE Biacore T200 machine located in the Biacore Facility, Duke University Human Vaccine Research Institute.

### 2.2 Single domain antibodies, cells culture conditions and animal model

Details of the production, purification and characterization of 2Rs15d sdAb have been reported [11, 28]. An anti-paraprotein sdAb R3B23 [7], which doesn't bind to HER2, was used for evaluating specificity of uptake. Both 2Rs15d and R3B23 are devoid of any tags such as a His-tag. Cell culture reagents were purchased from Thermo Fisher Scientific (Waltham, MA) except where noted. BT474M1 human breast carcinoma cells [29], a more tumorigenic version of the original BT474 line, were grown in RPMI1640 medium (Sigma-Aldrich, St. Louis, MO) containing 10 % fetal bovine serum, 1% penicillin-streptomycin, 1% non-essential amino acids, 1% sodium pyruvate, 1% 4-(2-hydroxyethyl)-1-piperazineethanesulfonic acid (HEPES) and 10μg/mL insulin (Sigma-Aldrich, St. Louis, MO). SKOV-3 human ovarian carcinoma cells, obtained from the Duke University Cell Culture Facility, were grown in McCoy's 5A medium containing 10% fetal bovine serum and 1% penicillin-streptomycin. Cells were cultured at 37°C in a 5% $CO_2$ humidified incubator. All experiments involving animals were performed using a protocol approved by the Duke University IACUC. Subcutaneous SKOV-3 xenografts were established by inoculating 10-week old female athymic mice, obtained from the Duke University, Division of Laboratory Animal Resources, with $5 \times 10^6$ SKOV-3 cells in 50% Matrigel (Corning Inc. NY) in the above medium (100 μL). The tumors were allowed to grow until they reached a volume of 350–500 $mm^3$ (~6–8 weeks).

### 2.3. N-succinimidyl 3-azidomethyl-5-guanidinomethylbenzoate (1)

A 95:2.5:2.5 (v/v/v) mixture of TFA:water:tri-isopropyl silane (0.25 mL) was added to *N*-succinimidyl 3-(azidomethyl)-5-((1,2-bis(*tert*-butoxycarbonyl)guanidino)methyl)benzoate [26] (29 mg; 0.05 mmol) and the mixture stirred at 20°C for 30 min. Solvents were evaporated and the residue re-dissolved in 0.25 mL of acetonitrile and subjected to semi-preparative HPLC purification. For this, the Poroshell EC-120 reversed-phase semi-preparative column was eluted at a flow rate of 4 mL/min with a gradient consisting of water (solvent A) and acetonitrile (solvent B); the proportion of B was increased from 5% to 15% in 20 min. Under these conditions the product eluted with a retention time of 13.9 min. Solvents from the pooled HPLC fractions were evaporated to get 19.5 mg (80% based on trifluoroacetate salt) of a clear oil. Analytical HPLC of the isolated product was performed using the analytical Poroshell column with flow rate of 2 mL/min with a gradient consisting of 0.1% formic acid in both water (solvent A) and acetonitrile (solvent B); the proportion of B was increased from 5% to 25% in 5 min. The product eluted with a retention time of 2.9 min and its purity was ~99%. $^1$H-NMR ($CD_3CN$) δ 2.85 (s, 4H), 4.43 (s, 2H), 4.52 (s, 2H), 7.67 (s, 1H), 8.00 (s, 1H), 8.01 (s, 1 H). LRMS (LCMS-ESI) *m/z*: 346.1 $(M+H)^+$. $^{13}$C-NMR ($CD_3CN$) δ 26.87, 45.09, 54.56, 127.16, 129.61, 130.26, 134.58, 139.62, 140.10, 158.94, 162.89, 171.53. HRMS (ESI) calcd for $C_{14}H_{15}N_7O_4$ $(M+H)^+$ 346.1583, found 346.1254 ± 0.0001 (n = 4).

### 2.4. 6-((Tert-butyldimethylsilyl)oxy)hexanoic acid (3)

This was synthesized essentially following the procedure reported previously [30]. Briefly, a mixture of *tert*-butyldimethylsilylchloride (1.84 g, 12.21 mmol), imidazole (816 mg, 11.99 mmol) and ethyl 6-hydroxyhexanoate (640 mg, 3.99 mmol) in DMF (10 mL) was stirred

under nitrogen at 20°C. After 24 h, the reaction mixture was diluted with ether (50 mL) and the ethereal solution washed with brine (150 mL × 3). The ether solution was separated, dried over $Na_2SO_4$, and the ether removed by rotary evaporation to obtain a yellow oil. A methanolic solution of Triton B (40% w/w, 10 mL) was added to this and the mixture stirred at 20°C for an hour. Methanol was removed under vacuum, water (20 mL) was added to the residue and the pH adjusted to 4 using 1M HCl. The aqueous phase was then extracted with ether (100 mL × 3) and the combined ether solution was dried over $Na_2SO_4$. Ether was evaporated to yield 609 mg (2.47 mmol, 61.9%) of compound **3** as a yellow oil: $^1$H-NMR ($CDCl_3$) δ 0.04 (s, 6H), 0.89 (s, 9H), 1.40 (dd, 2H), 1.53 (m, 2H), 1.65 (m, 2H), 3.61 (t, 2H).

### 2.5. Synthesis of compound 4 [27]

Compound **3** (187 mg, 0.76 mmol), EDC (58.3 mg, 0.30 mmol), and DMAP (3.1 mg, 0.03 mmol) were added to a solution of ADIBO-amine (70 mg, 0.25 mmol) in 5 mL DMF. The reaction mixture was stirred overnight at 20°C. The solvent was removed under vacuum and the residue dissolved in 50 mL dichloromethane. The resultant solution was washed with brine (3 × 50 mL), dried over $Na_2SO_4$, and dichloromethane removed using a rotary evaporator. The residue was purified by chromatography using 2% methanol in dichloromethane to obtain 100 mg (0.20 mmol, 78.2%) of compound **4** as a yellow oil: $^1$H-NMR ($CDCl_3$) δ 0.05 (s, 6H), 0.90 (s, 9H), 0.90 (s, 9H), 1.25–1.35 (m, 2H), 1.45 −1.55 (m, 4H), 1.95 – 2.05 (m, 3H), 2.40 – 2.50 (m, 1H), 3.27 – 3.37 (m, 2H), 3.60 (t, 2H), 3.70 (d, 1H), 5.15 (d, 1H), 6.00 (t, 1H), 7.26 – 7.42 (m, 7H), 7.68 (d, 1H). LRMS (LCMS-ESI) *m/z:* 505.2 $(M+H)^+$.

### 2.6. Synthesis of ADIBO-OTs (5) [27]

A mixture of compound **4** (100 mg, 0.20 mmol), tosyl fluoride (104 mg, 0.60 mmol) and DBU (15 μL, 0.10 mmol) in 3 mL of acetonitrile was stirred at 90°C for 2 h. The reaction mixture was cooled to 20°C, and partitioned between dichloromethane and brine (50 mL × 3). The pooled dichloromethane solution was dried with $Na_2SO_4$, and concentrated to dryness. The residue was taken up in acetonitrile and subjected to semi-preparative HPLC using the Agilent 1260 Infinity HPLC system. For this, an Agilent Poroshell EC-120 reversed-phase semi-preparative column was eluted with a gradient mobile phase consisting of 0.1% formic acid in both water (solvent A) and acetonitrile (solvent B) at a flow rate of 3 mL/min; the proportion of B was linearly increased from 40% to 70% over a period of 30 min. HPLC fractions containing the product ($t_R$ = 25 min) were pooled, and solvents evaporated to obtain 50 mg (0.09 mmol, 83%) of compound **5** as a colorless oil: $^1$H-NMR ($CDCl_3$) δ 1.22 – 1.32 (m, 2H), 1.40 – 1.47 (m, 2H), 1.58 – 1.65 (m, 2H), 1.90 – 1.97 (m, 3H), 2.41 – 2.47 (m, 1H), 2.45 (s, 3H), 3.18 – 3.37 (m, 2H), 3.68 (d, 1H), 4.01 (t, 2H), 5.12 (d, 1H), 5.97 (t, 1H), 7.25 – 7.40 (m,7H), 7.78 (d, 1H). LRMS (LCMS-ESI) *m/z:* 545.1 $(M+H)^+$.

### 2.7. Synthesis of F-ADIBO (6) [27]

Tetrabutyl ammonium fluoride (27 μL of 1M THF solution, 27 μmol) was added to a solution of **5** (5 mg, 9 μmol) in 1 mL of THF. The reaction mixture was refluxed for 30 min,

the solvent removed under vacuum, and the residue purified by RP-HPLC using the conditions described above to give 2.5 mg (6.4 μmol, 69%) of **6** ($t_R$ = 19 min) as a colorless oil: $^1$H-NMR ($CD_3CN$): 1.25 – 1.50 (m, 2H), 1.55 – 1.63 (m, 2H), 1.65 – 1.72 (m, 2H), 1.90 – 2.00 (m, 3H), 3.69 (d, 1H), 4.35 (t, 1H), 4.47 (t, 1H), 5.10 (d, 1H), 6.17 (t, 1H), 7.25 – 7.50 (m,7H), 7.66 (d, 1H). LRMS (LCMS-ESI) *m/z:* 393.2 $(M+H)^+$.

### 2.8. Synthesis of [$^{18}$F]F-ADIBO ([$^{18}$F]6)

ADIBO-[$^{18}$F]F was synthesized by slight modifications of a previously reported method [27]. Fluorine-18 was obtained either by in house cyclotron irradiation of [$^{18}$O]$H_2O$ as described before [26] or from PET-NET solutions (Durham, NC). For labeling reactions, $^{18}$F activity trapped in a QMA cartridge was eluted with 0.5 mL of a solution of tetraethylammonium bicarbonate in 80% acetonitrile (6 mg/mL) and dried by azeotroping with acetonitrile (3 × 1 mL). A solution of **5** (2 mg, 3.57 μmol) in 300 μL acetonitrile was added to the dried $^{18}$F activity (1.9 −3.7 GBq; 50–100 mCi), and heated at 100°C for 15 min. Acetonitrile was evaporated, and the residual activity dissolved in 100 μL of 40% acetonitrile and injected onto a Poroshell EC-120 column that was eluted under the conditions described above for **6**. The HPLC fractions containing [$^{18}$F]**6** were pooled and concentrated by solid-phase extraction using an Empore™ SPE cartridge (3M, St. Paul, MN) with acetonitrile (3 × 150 μL) as the eluent. Acetonitrile from the pooled fractions was evaporated and the activity reconstituted in PBS.

### 2.9. Derivatization of sdAbs with N-succinimidyl 3-azidomethyl-5-guanidinomethylbenzoate

A solution of the sdAb (2Rs15d or R3B23; 1.0 mg, ~0.08 μmol) in 0.1 M borate buffer, pH 8.5 (300 μL) was added to **1** (850 μg, 2.46 μmol) and the mixture stirred at 30°C for 2 h. The derivatized and non-derivatized sdAbs were isolated from unreacted reagent and borate salts by ultrafiltration using a Vivaspin® protein concentrator (5 kDa MWCO; GE Healthcare) and lyophilized to dryness. The molecular weight of sdAb conjugates was determined by MALDI-TOF mass spectrometry. The affinity for binding of the 2Rs15d conjugate to HER2 extracellular domain was determined by surface plasmon resonance (SPR).

### 2.10. Labeling derivatized sdAbs with $^{18}$F via SPAAC using [$^{18}$F]F-ADIBO

A solution of each sdAb (100 μL of 1 mg $mL^{-1}$) in PBS, pH 7.4 was added to a vial containing dried [$^{18}$F]F-ADIBO activity, and the mixture incubated at 20°C for 20 min. The entire mixture was loaded onto a PD-10 gel filtration column and eluted with PBS.

### 2.11. Determination of radiochemical purity

Three methods were used to determine the radiochemical purity/integrity of radiolabeled sdAbs: 1) To determine protein-associated activity, trichloroacetic acid precipitability was performed by incubating ~5 ng of the labeled sdAb with 300 μL of 1% human serum albumin (HSA) and 500 μL of 10% TCA in triplicate at 20°C for 1 min. 2) ITLC was done on silica gel-impregnated glass fiber sheets eluted with PBS (pH 7.4). The sheets were scanned by LabLogic Scan-RAM described above. The sdAbs remained at the origin and lower molecular weight species eluted with a retention factor of 0.47. 3) Non-reducing SDS-PAGE and subsequent phosphor imaging using a Storage Phosphor System Cyclone Plus

phosphor imager (Perkin-Elmer Life and Analytical Sciences, Downers Grove, IL) was used to assess the integrity of labeled proteins as previously described [16].

### 2.12. Determination of immunoreactivity and $K_d$ of [$^{18}$F]RL-II-2Rs15d

The immunoreactive fraction of [$^{18}$F]RL-II-2Rs15d was determined using the Lindmo method [31]. Briefly, streptavidin-coated magnetic beads (PureBiotech, Middlesex, NJ) were conjugated with the extracellular domain of HER2 (Acrobiosystems, Newark, DE), or to evaluate nonspecific binding, human serum albumin. Aliquots of [$^{18}$F]RL-II-2Rs15d (~5 ng) were incubated with increasing concentrations of both positive (HER2) and negative (HSA) beads. The reciprocal of the percentage of specific binding was plotted against the reciprocal of bead concentration and data were fit to a straight line by linear regression. The immunoreactive fraction was calculated as the reciprocal of the y-intercept value (binding at infinite antigen concentration).

For the saturation binding assay, BT474M1 cells were seeded in 24-well plates at a density of $8 \times 10^4$ cells/well/mL and incubated at 37°C overnight. Prior to the addition of [$^{18}$F]RL-II-2Rs15d, the cells were washed and replenished with fresh cold medium. Cells were then incubated with [$^{18}$F]RL-II-2Rs15d (0.1 to 300 nM; 0.6 mL/well) in triplicate at 4°C for 2 h, the medium containing unbound activity was removed, and the cells were washed twice with cold medium. Finally, the cells were lysed with 0.1% SDS and the activity in the cell lysate was counted using an automated gamma counter. To determine non-specific binding, parallel assays were performed as above but cells were co-incubated with a 100-fold excess of unlabeled 2Rs15d. The data were fit using GraphPad Prism software to determine $K_d$ values. The entire experiment was repeated thrice.

### 2.13. In vitro uptake assays

The cell uptake assay was performed in a paired-label format. BT474M1 cells ($8 \times 10^5$ cells per well/3 mL) were seeded in 6-well plates overnight at 37°C. The next day, the medium was replaced with 2 mL fresh medium containing 5 nM each of [$^{18}$F]RL-II-2Rs15d and [$^{125}$I]SGMIB-2Rs15d and the cells were incubated at 37°C for 1, 2, and 4 h. Then, the cell culture supernatants were removed, and the cells washed with medium ($2 \times 1$ mL) and lysed with SDS treatment. Activity in the cell culture supernatants and cell-associated fractions was counted in an automated gamma counter. To determine nonspecific uptake, a parallel experiment was performed as above but with the addition of a 100-fold molar excess of unlabeled 2Rs15d in the incubation media. The experiment was performed in triplicate and the entire experiment was repeated thrice.

### 2.14. Biodistribution

Paired-label biodistribution of [$^{18}$F]RL-II-2Rs15d and [$^{125}$I]SGMIB-2Rs15d was evaluated in SKOV-3 tumor bearing mice. Each mouse weighing about 25 g received 259 kBq (7 μCi, 1.7 μg) of [$^{18}$F]RL-II-2Rs15d and 185 kBq (5 μCi, 0.8 μg) of [$^{125}$I]SGMIB-2Rs15d in a total of 100 μL of PBS by bolus injection via the tail vein. Blood and urine were collected from groups of five mice, which were then killed and their tissues harvested at 1 and 2 h post injection. The isolated solid tissues were blot-dried, weighed, and the activity in them as well as in blood and urine was counted along with input standards. From these, the

percentage of the injected dose (ID) per organ and per gram of tissue (%ID/g) were calculated. Mouse thyroid being a very small organ, it is harvested with along with surrounding muscle tissue. The following formula was used to calculate the %ID/organ in the case of thyroid.

$$\%\,ID = \left(\left(\frac{n}{N}\right) * 100\right) - A * W\right)$$

*Where %ID is the percentage of injected dose in thyroid, n is the counts per minute obtained for thyroid and associated muscle combined, A is the %ID/g in muscle and W is the weight of thyroid and associated muscle*.

Statistical significance of the difference in uptake between the two radioisotopes was determined by a paired Student *t* test using Microsoft Excel program; a *P* value of <0.05 was considered to be significant.

### 2.15. MicroPET/CT imaging

Imaging of SKOV-3 subcutaneous xenograft-bearing mice was performed on a Siemens Inveon microPET/CT system (Knoxville, TN). Three mice were imaged 1 h, 2 h and 3 h after administration of 0.6 – 1.3 MBq (16 – 36 μCi; 3.7 – 8.3 μg) [$^{18}$F]RL-II-2Rs15d. Another two mice were imaged 1 h and 2 h after administration of 1.7 – 2.0 MBq (46 – 54 μCi; ~11.5 – 13.5 μg) [$^{18}$F]RL-II-R3B23. Mice were anesthetized using 2–3% isoflurane in oxygen and placed prone in the scanner gantry for a 5-min static PET acquisition followed by a 5 min CT scan. List mode PET data were histogram-processed, and the images reconstructed using the standard OSEM3D/MAP algorithm—2 OSEM3D iterations, and 18 MAP iterations—with a cutoff (Nyquist) of 0.5. Images were corrected for attenuation (CT-based) and radioactive decay. Image analysis was performed using Inveon Research Workplace software (Siemens).

## 3. Results and discussion

HER2-targeted vectors such as diabodies, affibodies and sdAbs labeled with $^{18}$F have been investigated for the determination of HER2 status by PET imaging [32–34]. Because of the short half-life, widespread availability and favorable radiation dosimetry properties of $^{18}$F, there is great interest in developing improved methods for labeling fast-clearing biomolecules with $^{18}$F that can be performed efficiently under physiological conditions. Of particular interest is the development of residualizing prosthetic moieties for labeling internalizing biomolecules with $^{18}$F because these can potentially augment tumor retention of activity after receptor-mediated internalization of the targeting vector occurs. In this regard, we developed a first-generation residualizing label via a click chemistry approach ([$^{18}$F]RL-I) and evaluated its potential utility for labeling two anti-HER2 sdAbs 5F7 and 2Rs15d [16, 34]. While excellent tumor targeting was seen with these tracers in HER2-expressing cells and xenografts, the labeling procedure was too long and labeling yields were too low for clinical translation. In an attempt to simplify the labeling procedure and potentially increase labeling efficiency, strain-promoted alkyne azide cycloaddition (SPAAC) was evaluated in the current study.

The azadibenzocyclooctyne (ADIBO)-based SPAAC partner reagent has been widely investigated in the past few years due to its good reactivity, stability and commercial availability. With a reduced activation barrier for SPAAC, azide-containing biomolecules such as peptides and proteins can be conveniently “clicked” with an ADIBO-containing reagent under physiological conditions. ADIBO-azide SPAAC has been used for site-specific conjugation of drugs to antibodies [35] and in live cell imaging [36] as well as in pre-targeting strategies [37]. Relevant to the work presented herein, ADIBO-azide SPAAC has been used for $^{18}$F-labeling of peptides and small molecules [38, 39] and recently, for labeling a protein [25].

Compound **1** (Scheme 1) was synthesized from its protected precursor [26] in about 80% yield. Its NMR and mass spectrometry characteristics were consistent with its structure. The precursor **5** and standard **6** (Scheme 2) were synthesized starting with commercially available **2** and known compound **3** [30] in two and three steps, respectively, following reported procedures [27]. The yields were similar to those reported with 78% for intermediate **4** (versus 87%), 83% for **5** (versus 83%) and 69% for **6** (versus 78%). NMR data for these compounds (as well as **3**) were consistent with their structures.

Conjugation of 2Rs15d with the azide- and residualizing guanidine-containing prosthetic agent (**1**) (Scheme 1) was accomplished in 70% yield when about 30 equivalents of the prosthetic agent were used; higher amounts of the prosthetic agent were precluded due to its poor water solubility. Although the addition of 3–5% DMSO was investigated, it failed to further improve the conjugation yield. MALDI-TOF mass spectrometry analysis revealed that about 70% of the 2Rs15d molecules were substituted with the prosthetic group with approximately 60%, 30% and 10% of these conjugated to one, two and three prosthetic groups, respectively. In the conjugation of **1** to control sdAb R3B23, about 35% of sdAb molecules were modified with one prosthetic group and another 15% with two prosthetic groups. Conjugating 2Rs15d with the prosthetic agent **1** did not affect its HER2 binding affinity (1.59 nM) measured by SPR (Figure 1A), which indicated a similar binding affinity as unmodified 2Rs15d (1.71 nM).

The decay-corrected radiochemical yield for the synthesis of [$^{18}$F]F-ADIBO ([$^{18}$F]**6**) was 55.9 ± 14.5% (n=8), and 23.9 ± 6.9% (n=8) for SPAAC between derivatized 2Rs15d and [$^{18}$F]F-ADIBO. The radiochemical yield for the synthesis of [$^{18}$F]F-ADIBO was somewhat lower than reported (65%) [27], which might reflect the use of a lower amount of precursor in our experiments (2 mg versus 7–9 mg). The total duration for synthesis of the [$^{18}$F]RL-II-2Rs15d conjugate was about 2 h and the overall decay-corrected radiochemical yield (based on the initial [$^{18}$F]fluoride activity) was 3.2 ± 0.9% (n = 8). With [$^{18}$F]RL-II-R3B23 control sdAb, the radiochemical yield for the conjugation reaction was 20.6% and the radiochemical purity was 97.2% by (ITLC).

It is known that the reaction rate constant for SPAAC is much lower than that for CuAAC ($k_2$ for CuAAC 10–100 $M^{-1}S^{-1}$ versus 0.001–0.96 $M^{-1}S^{-1}$ for SPAAC) [40]. Although higher $^{18}$F-labeling yields for SPAAC have been reported using similar systems, these studies involved low molecular weight azide-containing compounds including peptides for which the use of organic solvents and higher temperatures could be tolerated [27, 38]. It has

been demonstrated that addition of surfactants or organic solvents such as ethanol or acetonitrile, which may enhance the solubility of agents such as [$^{18}$F]F-ADIBO, can greatly improve the SPAAC reaction yield [40, 41]. However, use of organic solvents has been shown to be counterproductive in some cases [42]. In the current work, the use of higher incubation temperature (40°C), longer incubation time (up to 40 min), and addition of up to 5% DMSO were explored, but none of these tactics significantly increased the conjugation yield. Moreover, 2Rs15d sdAb precipitated at temperatures above 50°C or when more than 10% DMSO was added. It is highly likely that this may be due to derivatization with ADIBO as sdAbs including 2Rs15d [11] are known to be resistant to such conditions than intact antibodies. The utilization of SPAAC greatly simplified the labeling procedure, shortening the total radiosynthesis time to 2 h from 3 h required for labeling 2Rs15d with [$^{18}$F]RL-I via CuAAC [26]. However, the overall radiochemical yield was compromised due to low yield for the SPAAC reaction; thus there was no significant advantage compared with the [$^{18}$F]RL-I approach reported previously [26], at least with this particular combination of sdAb and ADIBO reagent. Comparison of labeling 2Rs15d with [$^{18}$F]RL-I and [$^{18}$F]RL-II is presented in Table 1.

As noted above, a recent publication has described $^{18}$F labeling of an Adnectin protein derivatized with a cyclooctyne moiety via SPAAC using an $^{18}$F-labeled azido compound [25]. While the authors did not give the radiochemical yield for SPAAC per se, the overall yield for the synthesis of $^{18}$F-labeled azido compound and its SPAAC reaction with cyclooctyne-derivatized Adnectin was about 3–4%, which was similar to the overall yield obtained in the current study. Given that the yield we obtained for [$^{18}$F]**6** was considerably lower than they obtained for their $^{18}$F-labeled azido compound (<50% vs >70%), the yield we obtained for the SPAAC reaction should be at least equal or perhaps better even though we were constrained to use a lower temperature for this reaction (20°C vs 45°C).

The specific activity of [$^{18}$F]RL-II-2Rs15d was in the range of 93 – 583 kBq/μg. SDS-PAGE/phosphor imaging of [$^{18}$F]RL-II-2Rs15d indicated a single radioactive band, which corresponded to the molecular weight of 2Rs15d (Figure 1B). The radiochemical purity of [$^{18}$F]RL-II-2Rs15d was further demonstrated by ITLC (95.5 ± 1.8%) and TCA precipitability (98.4 ± 0.1%). The immunoreactive fraction determined by Lindmo assay for [$^{18}$F]RL-II-2Rs15d was 70.4% (Figure 1C) and a $K_d$ value of 5.6 ± 1.3 nM was measured by saturation binding assay on HER2-expressing BT474M1 cells (Figure 1D). These data indicate that labeling 2Rs15d using [$^{18}$F]RL-II-2Rs15d did not significantly affect its binding to HER2 and this is consistent with the fact that none of the lysines in 2Rs15d is in the HER2 binding region [9].

The uptake of [$^{18}$F]RL-II-2Rs15d and [$^{125}$I]SGMIB-2Rs15d by BT474M1 human breast carcinoma cells in vitro was determined in a paired-label format. As shown in Figure 2, about 14–17% of the added [$^{18}$F]RL-II-2Rs15d was specifically bound to the cells over 1–4 h. The uptake was similar to that observed for co-incubated [$^{125}$I]SGMIB-2Rs15d ($P > 0.05$) at 1 and 2 h and slightly higher ($P < 0.01$) at 4 h. These results confirm that substitution of the prosthetic moiety onto 2Rs15d and the reaction conditions used for labeling this sdAb using the [$^{18}$F]RL-II approach did not affect its binding and internalization to HER2-positive cancer cells. Furthermore, the results suggest that the degree of residualization of activity in

tumor cells in vitro achieved with [$^{18}$F]RL-II was similar to that obtained with the prototypical residualization agent SGMIB. These results cannot be directly compared with those reported earlier for [$^{18}$F]RL-I-2Rs15d [16] because the assay format was different in the two cases. In the current study, cells were incubated at 37°C with the labeled sdAb and cell-associated activity determined and expressed as percent of initially added activity. On the other hand, in the previous study, the cells were incubated initially at 4°C and after removing the medium containing unbound activity, cells were incubated with fresh medium at 37°C, with surface-bound and internalized activity determined and expressed as the percent of initially bound activity in these compartments. However, the 14–17% specific uptake observed on BT474M1 cells for [$^{18}$F]RL-II-2Rs15d was similar to total uptake reported for 2Rs15d radiolabeled using a sortase-based approach and assayed under similar conditions [43]. For example, after 1 h incubation, the percent of input dose bound to cells was about 16–17% for [$^{111}$In]In-CHX-A”-DTPA-2Rs15d and about 11–14% for $^{68}$Ga-NOTA-2Rs15d. It is worth pointing out that in that study, 2Rs15d was labeled with radiometal-containing chelates, which are generally considered to be residualizing prosthetic agents, further supporting the residualizing character of the [$^{18}$F]RL-II prosthetic agent.

The results obtained from the biodistribution of [$^{18}$F]RL-II-2Rs15d and [$^{125}$I]SGMIB-2Rs15d at 1, and 2 h post injection are summarized in Table 2. The tumor uptake of [$^{18}$F]RL-II-2Rs15d was 5.54 ± 0.77 %ID/g at 1 h and 6.42 ± 1.70 %ID/g at 2 h ($P$ > 0.05). Although these values were higher than those observed for co-injected [$^{125}$I]SGMIB-2Rs15d, the differences between the two radioconjugates were not statistically significant ($P$ > 0.05). The tumor uptake of [$^{18}$F]RL-II-2Rs15d was significantly lower than observed previously with [$^{18}$F]RL-I-2Rs15d (15–20 %ID/g) [16]; however, it should be noted that BT474M1 xenografts were used in the earlier study. Although there are conflicting reports concerning the relative receptor number per cell for these two lines [44, 45], it appears that the BT474 cell line expresses HER2 to a higher degree [28, 45]. Concordant with this, we have consistently seen high tumor uptake (>10% ID/g) for various radiolabeled sdAbs in the BT474M1 xenograft model [34, 46, 47]. Other radiolabeled 2Rs15d conjugates have been evaluated in mice with SKOV-3 xenografts [11, 28, 48–50], providing more relevant benchmarks for comparison. The tumor uptake observed for [$^{18}$F]RL-II-2Rs15d in SKOV-3 xenografts compared favorably with the values reported for these other radiolabeled sdAb conjugates both in terms of peak tumor uptake and retention of activity in the xenograft. In most of the studies mentioned above, 2Rs15d was labeled with residualizing, radiometal-bearing prosthetic agents. On the other hand, when 2Rs15d was labeled with the non-residualizing [$^{18}$F]SFB agent, tumor uptake decreased significantly from 1 h (5.94 ± 1.17 %IA/g) to 3 h (3.74 ± 0.52) [50]. These comparisons to literature data performed with the same sdAb and the same tumor model suggest a potential tumor delivery advantage for using the residualizing [$^{18}$F]RL-II prosthetic agent for labeling sdAbs that target internalizing receptors such as HER2.

Both radiolabeled sdAbs demonstrated rapid clearance, with <1% ID/g in the blood even at 1 h. Clearance of both radioconjugates occurred mainly through the kidneys, which was expected because the ~15 kDa size of sdAb is below the cutoff for renal filtration of proteins (~60 kDa) [51]. There was a slight advantage in tumor uptake for 2Rs15d labeled using [$^{18}$F]RL-II; however, its uptake in normal tissues such as liver, spleen and kidney was

substantially higher than that seen for [$^{125}$I]SGMIB-2Rs15d. As a result of the higher uptake in normal tissues for [$^{18}$F]RL-II-2Rs15d, tumor-to-tissue ratios were considerably lower for the $^{18}$F-labeled construct (Table 3).

The relatively bulky and hydrophobic cyclooctyne moiety present in RL-II has been reported to significantly influence the biodistribution properties of its bioconjugates [52]. This may be a contributing factor for the higher normal tissue uptake observed for [$^{18}$F]RL-II-2Rs15d compared with [$^{125}$I]SGMIB-2Rs15d. Of note, kidney uptake of [$^{18}$F]RL-II-2Rs15d was more than 3-fold higher than that seen for [$^{125}$I]SGMIB-2Rs15d, which was unexpected given the hydrophobic nature of the cyclooctyne moiety. Although the high renal uptake observed with [$^{18}$F]RL-II-2Rs15d is consistent with the molecular weight of an sdAb, the reasons that its kidney uptake was considerably higher than co-injected [$^{125}$I]SGMIB-2Rs15d are unclear. The highly basic guanidine moiety is present in both [$^{18}$F]RL-II and [$^{125}$I]SGMIB, so it is probably not a factor. On the other hand, a triazole and the bulky cyclooctyne moieties are present only in [$^{18}$F]RL-II-2Rs15d, and thus might have contributed to higher renal uptake of [$^{18}$F]RL-II-2Rs15d. While there are conflicting reports on the influence of triazoles on the uptake of activity in kidneys and other normal tissues, a direct comparison of folic acid conjugates with and without a triazole moiety showed significantly higher renal uptake for the conjugate with the triazole [53]. Finally, kidney uptake of [$^{18}$F]fluoride is well documented [54, 55], and [$^{18}$F]fluoride generated by the catabolism of [$^{18}$F]RL-II-2Rs15d (see below) also might have contributed to high kidney uptake.

The uptake of [$^{18}$F]RL-II-2Rs15d in the bone at 1 h was more than 1.4-fold higher than that observed with [$^{18}$F]RL-I-2Rs15d in the BT474M1 xenograft model [16] and about 7-fold higher than that reported for 2Rs15d labeled using [$^{18}$F]SFB in SKOV-3 xenograft model [50]. Furthermore, bone uptake increased from 1 h to 2 h suggesting that 2Rs15d labeled using [$^{18}$F]RL-II may be more susceptible to defluorination than when labeled using the other two prosthetic moieties. When an sdAb that targets the complement receptor of the Ig super family was labeled with $^{18}$F via the [$^{18}$F][AlF]$^{2+}$ method, bone uptake increased with time, which was attributed to degradation of the labeled sdAb in kidney lysosomes and recycling of [$^{18}$F]fluroride and [$^{18}$F][AlF]$^{2+}$ [54]. We speculate that [$^{18}$F]RL-II-2Rs15d also may be subjected to this phenomenon generating more [$^{18}$F]fluroride; however, it appears that the [$^{18}$F]RL-II method is more inert to defluorination than [$^{18}$F][AlF]$^{2+}$ method. It has been reported that the internalization of two anti-HER2 scFv-HSA fusion proteins was different in BT474 and SKOV-3 cells [56]. Given this, it is also possible that internalization, trapping, and in turn the metabolism of the labeled sdAbs may be different for BT474M1 and SKOV-3 cells, which also may have contributed to differential bone uptake.

Although two different xenograft models were used in the current and the previous [16] studies evaluating potential $^{18}$F-labeled residualizing prosthetic agents, in both cases, the biodistribution of co-injected [$^{125}$I]SGMIB-2Rs15d also was determined. Thus, it is possible to compare the biodistributions of [$^{18}$F]RL-II-2Rs15d and [$^{18}$F]RL-I-2Rs15d, by normalizing to co-injected [$^{125}$I]SGMIB-2Rs15d through calculation of $^{18}$F/$^{125}$I tissue uptake ratios. As shown in Table 4, [$^{18}$F]RL-II is favored over [$^{18}$F]RL-I providing relatively higher tumor uptake, as well as lower uptake in liver, spleen and lungs. On the other hand,

compared with [$^{18}$F]RL-I, [$^{18}$F]RL-II labeling results in relatively higher uptake in other normal tissues including brain, bone and kidneys. Because breast cancers are known to metastasize to liver, lungs, brain and bone, [$^{18}$F]RL-II may the more useful approach for evaluating metastatic spread in the liver and lungs, but not brain and bone. Ideally, next generation [$^{18}$F]RL-II derivatives can be designed with structures that decrease defluorination and minimize uptake in the bone and other normal tissues.

Coronal PET/CT images obtained 1, 2 and 3 h after administration of [$^{18}$F]RL-II-2Rs15d in a representative athymic mouse bearing a subcutaneous SKOV-3 xenograft are depicted in Figure 3A. Concordant with the data from the necropsy experiment, clear delineation of tumor was observed with minimal background activity in normal tissues except in kidneys, which exhibited prominent and prolonged uptake. That the tumor uptake was related to specific binding to HER2 was demonstrated by the absence of activity accumulation in the tumor after injection of nonspecific [$^{18}$F]RL-II-R3B23 (Figure 3B). The tumor-to-muscle ratios for [$^{18}$F]RL-II-2Rs15d (n = 3) were 9.6 ± 1.7, 11.5 ± 2.3, and 20.9 ± 2.1 at 1 h, 2 h, and 3 h, respectively. The values at 1 h and 2 h were similar to that obtained from the necropsy experiment. For [$^{18}$F]RL-II-R3B23 (n = 2) tumor-to-muscle ratios were 1.8 ± 0.4 and 1.8 ± 0.1 at 1 h and 2 h, respectively.

## 4. Conclusion

Although SPAAC has been used to label peptides, other small molecules, and in one case the protein Adnectin, to our knowledge, this is the first study evaluating its utility for labeling an sdAb with $^{18}$F. When labeled using [$^{18}$F]RL-II, sdAb 2Rs15d demonstrated excellent affinity and immunoreactivity for HER2, and uptake comparable to [$^{125}$I]SGMIB-2Rs15d in vitro in HER2-expressing BT474M1 cells. Moreover, in athymic mice with HER2-expressing SKOV-3 xenografts, tumor uptake was virtually identical to [$^{125}$I]SGMIB-2Rs15d and compared favorably to those reported in the literature for 2Rs15d radioimmunoconjugates including those labeled with radiometals. To make this labeling strategy more attractive, it will be necessary to improve SPAAC yields or adapt other biorthogonal chemistry approaches that provide higher radiochemical yields, and to develop labeled sdAb with greater in vivo stability and lower normal tissue accumulation.

## Supplementary Material

Refer to Web version on PubMed Central for supplementary material.

## Acknowledgments

This work was supported in part by National Institutes of Health Grants CA188177 and CA42324. The excellent technical assistance of Elzbieta Krol (in vitro studies) and Xiao-Guang Zhao (in vivo studies) is greatly appreciated. We also thank Thomas Hawk, and Simone Degan for their excellent support with microPET/CT imaging studies.

## Abbreviations

| | |
|---|---|
| **sdAb** | single domain antibody fragment |
| **CuAAC** | copper-catalyzed azide-alkyne cycloaddition |

| | |
|---|---|
| **SPAAC** | strain-promoted azide-alkyne cycloaddition |
| **SGMIB** | *N*-succinimidyl 4-guanidinomethyl-3-iodobenzoate |
| **RCP** | radiochemical purity |
| **ADIBO** | aza-dibenzocyclooctyne |
| **PET** | positron emission tomography |

## References


1. Gainkam LO, Huang L, Caveliers V, Keyaerts M, Hernot S, Vaneycken I, Vanhove C, Revets H, De Baetselier P, Lahoutte T. Comparison of the biodistribution tumor targeting of two 99mTc-labeled anti-EGFR nanobodies in mice, using pinhole SPECT/micro-CT. J Nucl Med. 2008; 49:788–795. [PubMed: 18413403]
2. Roovers RC, Laeremans T, Huang L, De Taeye S, Verkleij AJ, Revets H, de Haard HJ, van Bergen en Henegouwen PM. Efficient inhibition of EGFR signaling and of tumour growth by antagonistic anti-EFGR nanobodies. Cancer Immunol Immunother. 2007; 56:303–317. [PubMed: 16738850]
3. Roovers RC, Vosjan MJ, Laeremans T, el Khoulati R, de Bruin RC, Ferguson KM, Verkleij AJ, van Dongen GA, van Bergen en Henegouwen PM. A biparatopic anti-EGFR nanobody efficiently inhibits solid tumour growth. Int J Cancer. 2011; 129:2013–2024. [PubMed: 21520037]
4. Evazalipour M, D'Huyvetter M, Tehrani BS, Abolhassani M, Omidfar K, Abdoli S, Arezumand R, Morovvati H, Lahoutte T, Muyldermans S, Devoogdt N. Generation and characterization of nanobodies targeting PSMA for molecular imaging of prostate cancer. Contrast Media Mol Imaging. 2014; 9:211–220. [PubMed: 24700748]
5. Fan X, Wang L, Guo Y, Tu Z, Li L, Tong H, Xu Y, Li R, Fang K. Ultrasonic nanobubbles carrying anti-PSMA nanobody: construction and application in prostate cancer-targeted imaging. PLoS One. 2015; 10:e0127419. [PubMed: 26111008]
6. Zare H, Rajabibazl M, Rasooli I, Ebrahimizadeh W, Bakherad H, Ardakani LS, Gargari SL. Production of nanobodies against prostate-specific membrane antigen (PSMA) recognizing LnCaP cells. Int J Biol Markers. 2014; 29:e169–179. [PubMed: 24425321]
7. Lemaire M, D'Huyvetter M, Lahoutte T, Van Valckenborgh E, Menu E, De Bruyne E, Kronenberger P, Wernery U, Muyldermans S, Devoogdt N, Vanderkerken K. Imaging and radioimmunotherapy of multiple myeloma with anti-idiotypic nanobodies. Leukemia. 2014; 28:444–447. [PubMed: 24166214]
8. Slordahl TS, Denayer T, Moen SH, Standal T, Borset M, Ververken C, Ro TB. Anti-c-MET nanobody - a new potential drug in multiple myeloma treatment. Eur J Haematol. 2013; 91:399–410. [PubMed: 23952536]
9. D'Huyvetter M, De Vos J, Xavier C, Pruszynski M, Sterckx YGJ, Massa S, Raes G, Caveliers V, Zalutsky M, Lahoutte T, Devoogdt N. $^{131}$I-labeled anti-HER2 camelid sdAb as a theranostic tool in cancer treatment. Clin Cancer Res. 2017; 23:6616–6628. [PubMed: 28751451]
10. Keyaerts M, Xavier C, Heemskerk J, Devoogdt N, Everaert H, Ackaert C, Vanhoeij M, Duhoux FP, Gevaert T, Simon P, Schallier D, Fontaine C, Vaneycken I, Vanhove C, De Greve J, Lamote J, Caveliers V, Lahoutte T. Phase I study of $^{68}$Ga-HER2-nanobody for PET/CT assessment of HER2 expression in breast carcinoma. J Nucl Med. 2016; 57:27–33. [PubMed: 26449837]
11. Vaneycken I, Devoogdt N, Van Gassen N, Vincke C, Xavier C, Wernery U, Muyldermans S, Lahoutte T, Caveliers V. Preclinical screening of anti-HER2 nanobodies for molecular imaging of breast cancer. Faseb J. 2011; 25:2433–2446. [PubMed: 21478264]
12. Carlsson J, Nordgren H, Sjostrom J, Wester K, Villman K, Bengtsson NO, Ostenstad B, Lundqvist H, Blomqvist C. HER2 expression in breast cancer primary tumours and corresponding metastases. Original data and literature review. Br J Cancer. 2004; 90:2344–2348. [PubMed: 15150568]

13. Yan M, Schwaederle M, Arguello D, Millis SZ, Gatalica Z, Kurzrock R. HER2 expression status in diverse cancers: review of results from 37,992 patients. Cancer Metastasis Rev. 2015; 34:157–164. [PubMed: 25712293]
14. Vaidyanathan G, Zalutsky MR. Synthesis of *N*-succinimidyl 4-guanidinomethyl-3-[*I]iodobenzoate: a radio-iodination agent for labeling internalizing proteins and peptides. Nat Protoc. 2007; 2:282–286. [PubMed: 17406587]
15. Boswell CA, Marik J, Elowson MJ, Reyes NA, Ulufatu S, Bumbaca D, Yip V, Mundo EE, Majidy N, Van Hoy M, Goriparthi SN, Trias A, Gill HS, Williams SP, Junutula JR, Fielder PJ, Khawli LA. Enhanced tumor retention of a radiohalogen label for site-specific modification of antibodies. J Med Chem. 2013; 56:9418–9426. [PubMed: 24131491]
16. Zhou Z, Vaidyanathan G, McDougal D, Kang CM, Balyasnikova I, Devoogdt N, Ta AN, McNaughton BR, Zalutsky MR. Fluorine-18-labeling of the HER2-targeting single domain antibody 2Rs15d using a residualizing label and preclinical evaluation. Mol Img Biol. 2017; 19:867–877.
17. Gill HS, Tinianow JN, Ogasawara A, Flores JE, Vanderbilt AN, Raab H, Scheer JM, Vandlen R, Williams SP, Marik J. A modular platform for the rapid site-specific radiolabeling of proteins with $^{18}$F exemplified by quantitative positron emission tomography of human epidermal growth factor receptor 2. J Med Chem. 2009; 52:5816–5825. [PubMed: 19736996]
18. Ramenda T, Kniess T, Bergmann R, Steinbach J, Wuest F. Radiolabelling of proteins with fluorine-18 via click chemistry. Chem Commun. 2009:7521–7523.
19. Wang L, Jacobson O, Avdic D, Rotstein BH, Weiss ID, Collier L, Chen X, Vasdev N, Liang SH. Ortho-stabilized $^{18}$F-azido click agents and their application in PET Imaging with single-stranded DNA aptamers. Angew Chem Int Ed Engl. 2015; 54:12777–12781. [PubMed: 26308650]
20. Kim DW. Bioorthogonal click chemistry for fluorine-18 labeling protocols under physiologically friendly reaction condition. J Fluorine Chem. 2015; 174:142–147.
21. Baskin JM, Prescher JA, Laughlin ST, Agard NJ, Chang PV, Miller IA, Lo A, Codelli JA, Bertozzi CR. Copper-free click chemistry for dynamic in vivo imaging. Proc Natl Acad Sci USA. 2007; 104:16793–16797. [PubMed: 17942682]
22. Demeter O, Fodor EA, Kallay M, Mezo G, Nemeth K, Szabo PT, Kele P. A double-clicking bis-azide fluorogenic dye for bioorthogonal self-labeling peptide tags. Chemistry A Eur J. 2016; 22:6382–6388.
23. Jang S, Sachin K, Lee HJ, Kim DW, Lee HS. Development of a simple method for protein conjugation by copper-free click reaction and its application to antibody-free Western blot analysis. Bioconjug Chem. 2012; 23:2256–2261. [PubMed: 23039792]
24. Rashidian M, Wang L, Edens JG, Jacobsen JT, Hossain I, Wang Q, Victora GD, Vasdev N, Ploegh H, Liang SH. Enzyme-mediated modification of single-domain antibodies for imaging modalities with different characteristics. Angew Chem Int Ed Engl. 2016; 55:528–533. [PubMed: 26630549]
25. Donnelly DJ, Smith RA, Morin P, Lipovsek D, Gokemeijer J, Cohen D, Lafont V, Tran T, Cole EL, Wright M, Kim J, Pena A, Kukral D, Dischino DD, Chow P, Gan J, Adelakun O, Wang XT, Cao K, Lueng D, Bonacorsi S Jr, Hayes W. Synthesis and biological evaluation of a novel $^{18}$F-labeled adnectin as a PET radioligand for imaging PD-L1 expression. J Nucl Med. 2017; doi: 10.2967/jnumed.117.199596
26. Vaidyanathan G, McDougald D, Choi J, Pruszynski M, Koumarianou E, Zhou Z, Zalutsky MR. *N*-Succinimidyl 3-((4-(4-[$^{18}$F]fluorobutyl)-1H-1,2,3-triazol-1-yl)methyl)-5-(guanidinomethyl)benzoate ([$^{18}$F]SFBTMGMB): a residualizing label for $^{18}$F-labeling of internalizing biomolecules. Org Biomol Chem. 2016; 14:1261–1271. [PubMed: 26645790]
27. Arumugam S, Chin J, Schirrmacher R, Popik VV, Kostikov AP. [$^{18}$F]azadibenzocyclooctyne ([$^{18}$F]ADIBO): a biocompatible radioactive labeling synthon for peptides using catalyst free [3+2] cycloaddition. Bioorg Med Chem Lett. 2011; 21:6987–6991. [PubMed: 22024032]
28. Xavier C, Vaneycken I, D'Huyvetter M, Heemskerk J, Keyaerts M, Vincke C, Devoogdt N, Muyldermans S, Lahoutte T, Caveliers V. Synthesis preclinical validation, dosimetry, and toxicity of $^{68}$Ga-NOTA-Anti-HER2 nanobodies for iPET imaging of HER2 receptor expression in cancer. J Nucl Med. 2013; 54:776–784. [PubMed: 23487015]

29. Yu Z, Xia W, Wang HY, Wang SC, Pan Y, Kwong KY, Hortobagyi GN, Hung MC. Antitumor activity of an Ets protein, PEA3, in breast cancer cell lines MDA-MB-361DYT2 and BT474M1. Mol Carcinog. 2006; 45:667–675. [PubMed: 16652376]
30. Su M, Wang J, Tang X. Photocaging strategy for functionalisation of oligonucleotides and its applications for oligonucleotide labelling and cyclisation. Chemistry A Eur J. 2012; 18:9628–9637.
31. Lindmo T, Boven E, Cuttitta F, Fedorko J, Bunn PA Jr. Determination of the immunoreactive fraction of radiolabeled monoclonal antibodies by linear extrapolation to binding at infinite antigen excess. J Immunol Methods. 1984; 72:77–89. [PubMed: 6086763]
32. Olafsen T, Sirk SJ, Olma S, Shen CK, Wu AM. ImmunoPET using engineered antibody fragments: fluorine-18 labeled diabodies for same-day imaging. Tumour Biol. 2012; 33:669–677. [PubMed: 22392499]
33. Trousil S, Hoppmann S, Nguyen QD, Kaliszczak M, Tomasi G, Iveson P, Hiscock D, Aboagye EO. Positron emission tomography imaging with $^{18}$F-Labeled ZHER2:2891 affibody for detection of HER2 expression and pharmacodynamic response to HER2-modulating therapies. Clin Cancer Res. 2014; 20:1632–1643. [PubMed: 24493830]
34. Vaidyanathan G, McDougald D, Choi J, Koumarianou E, Weitzel D, Osada T, Lyerly HK, Zalutsky MR. Preclinical evaluation of $^{18}$F-labeled anti-HER2 nanobody conjugates for imaging HER2 receptor expression by immuno-PET. J Nucl Med. 2016; 57:967–973. [PubMed: 26912425]
35. Zimmerman ES, Heibeck TH, Gill A, Li X, Murray CJ, Madlansacay MR, Tran C, Uter NT, Yin G, Rivers PJ, Yam AY, Wang WD, Steiner AR, Bajad SU, Penta K, Yang W, Hallam TJ, Thanos CD, Sato AK. Production of site-specific antibody-drug conjugates using optimized non-natural amino acids in a cell-free expression system. Bioconjug Chem. 2014; 25:351–361. [PubMed: 24437342]
36. Yao JZ, Uttamapinant C, Poloukhtine A, Baskin JM, Codelli JA, Sletten EM, Bertozzi CR, Popik VV, Ting AY. Fluorophore targeting to cellular proteins via enzyme-mediated azide ligation and strain-promoted cycloaddition. J Am Chem Soc. 2012; 134:3720–3728. [PubMed: 22239252]
37. Rossin R, Robillard MS. Pretargeted imaging using bioorthogonal chemistry in mice. Curr Opin Chem Biol. 2014; 21:161–169. [PubMed: 25159021]
38. Bouvet V, Wuest M, Wuest F. Copper-free click chemistry with the short-lived positron emitter fluorine-18. Org Biomol Chem. 2011; 9:7393–7399. [PubMed: 21938294]
39. Kettenbach K, Ross TL. A F-18-labeled dibenzocyclooctyne (DBCO) derivative for copper-free click labeling of biomolecules. Medchem Commun. 2016; 7:654–657.
40. Anderton GI, Bangerter AS, Davis TC, Feng Z, Furtak AJ, Larsen JO, Scroggin TL, Heemstra JM. Accelerating strain-promoted azide-alkyne cycloaddition using micellar catalysis. Bioconjug Chem. 2015; 26:1687–1691. [PubMed: 26056848]
41. Dommerholt J, Rutjes FPJT, van Delft FL. Strain-promoted 1,3-dipolar cycloaddition of cycloalkynes and organic azides. Topics Curr Chem. 2016; 374doi: 10.1007/s41061-016-0016-4
42. Davis DL, Price EK, Aderibigbe SO, Larkin MX, Barlow ED, Chen R, Ford LC, Gray ZT, Gren SH, Jin Y, Keddington KS, Kent AD, Kim D, Lewis A, Marrouche RS, O'Dair MK, Powell DR, Scadden MH, Session CB, Tao J, Trieu J, Whiteford KN, Yuan Z, Yun G, Zhu J, Heemstra JM. Effect of buffer conditions and organic cosolvents on the rate of strain-promoted azide-alkyne cycloaddition. J Org Chem. 2016; 81:6816–6819. [PubMed: 27387821]
43. Massa S, Vikani N, Betti C, Ballet S, Vanderhaegen S, Steyaert J, Descamps B, Vanhove C, Bunschoten A, van Leeuwen FW, Hernot S, Caveliers V, Lahoutte T, Muyldermans S, Xavier C, Devoogdt N. Sortase A-mediated site-specific labeling of camelid single-domain antibody-fragments: a versatile strategy for multiple molecular imaging modalities. Contrast Media Mol Img. 2016; 11:328–339.
44. Honarvar H, Westerlund K, Altai M, Sandstrom M, Orlova A, Tolmachev V, Karlstrom AE. Feasibility of affibody molecule-based PNA-mediated radionuclide pretargeting of malignant tumors. Theranostics. 2016; 6:93–103. [PubMed: 26722376]
45. Tolmachev V. Imaging of HER-2 overexpression in tumors for guiding therapy. Curr Pharm Des. 2008; 14:2999–3019. [PubMed: 18991715]
46. Pruszynski M, Koumarianou E, Vaidyanathan G, Revets H, Devoogdt N, Lahoutte T, Lyerly HK, Zalutsky MR. Improved tumor targeting of anti-HER2 nanobody through *N*-succinimidyl 4-

guanidinomethyl-3-iodobenzoate radiolabeling. J Nucl Med. 2014; 55:650–656. [PubMed: 24578241]

47. Choi J, Vaidyanathan G, Koumarianou E, Kang CM, Zalutsky MR. Astatine-211 labeled anti-HER2 5F7 single domain antibody fragment conjugates: radiolabeling and preliminary evaluation. Nucl Med Biol. 2017; 56:10–20. [PubMed: 29031230]
48. D'Huyvetter M, Aerts A, Xavier C, Vaneycken I, Devoogdt N, Gijs M, Impens N, Baatout S, Ponsard B, Muyldermans S, Caveliers V, Lahoutte T. Development of $^{177}$Lu-nanobodies for radioimmunotherapy of HER2-positive breast cancer: evaluation of different bifunctional chelators. Contrast Media Mol Img. 2012; 7:254–264.
49. D'Huyvetter M, Vincke C, Xavier C, Aerts A, Impens N, Baatout S, De Raeve H, Muyldermans S, Caveliers V, Devoogdt N, Lahoutte T. Targeted radionuclide therapy with A $^{177}$Lu-labeled anti-HER2 nanobody. Theranostics. 2014; 4:708–720. [PubMed: 24883121]
50. Xavier C, Blykers A, Vaneycken I, D'Huyvetter M, Heemskerk J, Lahoutte T, Devoogdt N, Caveliers V. $^{18}$F-nanobody for PET imaging of HER2 overexpressing tumors. Nucl Med Biol. 2016; 43:247–252. [PubMed: 27067045]
51. Vegt E, de Jong M, Wetzels JF, Masereeuw R, Melis M, Oyen WJ, Gotthardt M, Boerman OC. Renal toxicity of radiolabeled peptides and antibody fragments: mechanisms, impact on radionuclide therapy, and strategies for prevention. J Nucl Med. 2010; 51:1049–1058. [PubMed: 20554737]
52. McKay CS, Finn MG. Click chemistry in complex mixtures: bioorthogonal bioconjugation. Chem Biol. 2014; 21:1075–1101. [PubMed: 25237856]
53. Reber J, Struthers H, Betzel T, Hohn A, Schibli R, Muller C. Radioiodinated folic acid conjugates: evaluation of a valuable concept to improve tumor-to-background contrast. Mol Pharm. 2012; 9:1213–1221. [PubMed: 22509996]
54. Cleeren F, Lecina J, Ahamed M, Raes G, Devoogdt N, Caveliers V, McQuade P, Rubins DJ, Li W, Verbruggen A, Xavier C, Bormans G. Al$^{18}$F-labeling of heat-sensitive biomolecules for positron emission tomography imaging. Theranostics. 2017; 7:2924–2939. [PubMed: 28824726]
55. Schnockel U, Reuter S, Stegger L, Schlatter E, Schafers KP, Hermann S, Schober O, Gabriels G, Schafers M. Dynamic $^{18}$F-fluoride small animal PET to noninvasively assess renal function in rats. Eur J Nucl Med Mol Imaging. 2008; 35:2267–2274. [PubMed: 18622612]
56. Zhang H, Wang Y, Wu Y, Jiang X, Tao Y, Yao Y, Peng Y, Chen X, Fu Y, Yu L, Wang R, Lai Q, Lai W, Li W, Kang Y, Yi S, Lu Y, Gou L, Wu M, Yang J. Therapeutic potential of an anti-HER2 single chain antibody–DM1 conjugates for the treatment of HER2-positive cancer. Signal Transduction and Targeted Therapy. 2017; 2:e17015.doi: 10.1038/sigtrans.2017.15

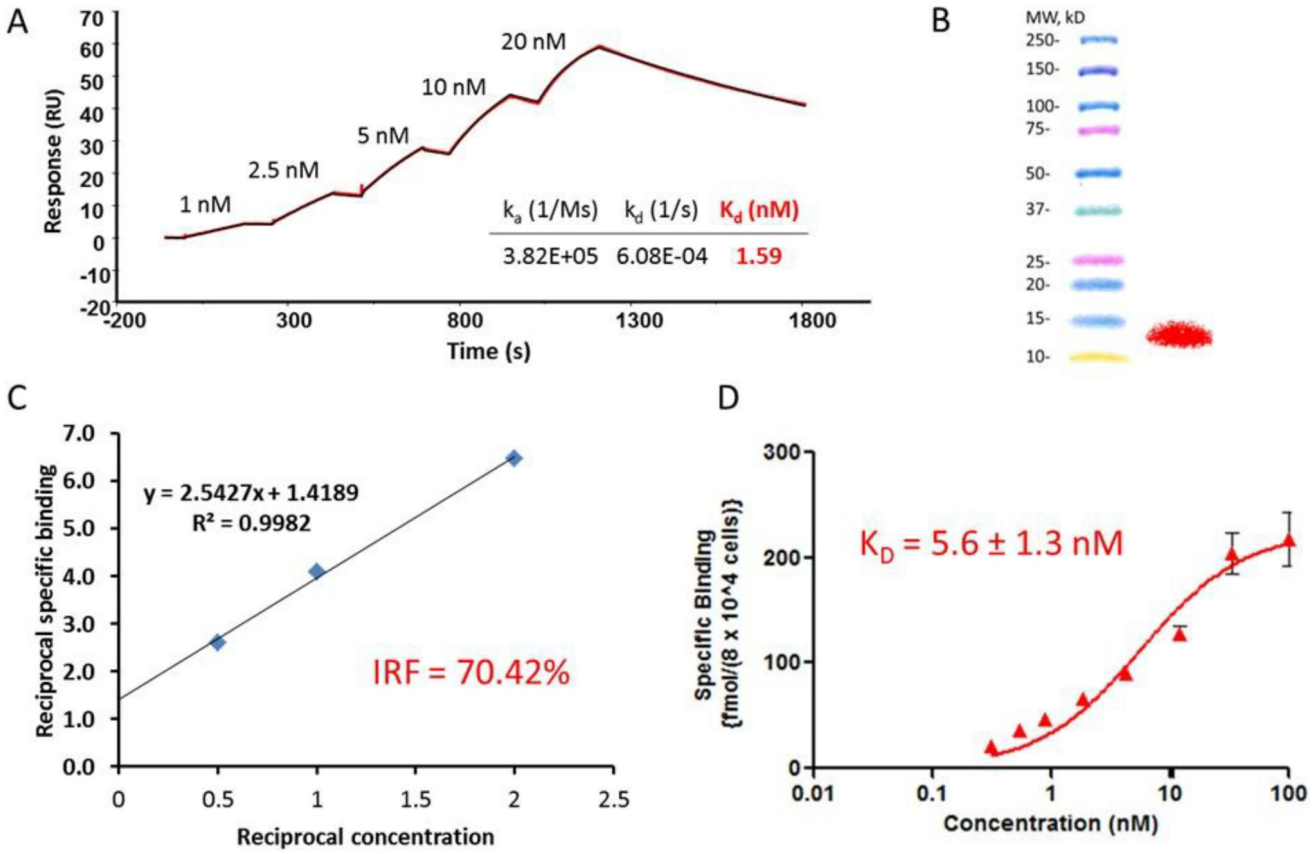


**Figure 1.**

In vitro quality control data for preconjugated 2Rs15d and [$^{18}$F]RL-II-2Rs15d. A) Surface Plasmon Resonance analysis. B) SDS-PAGE/phosphor imaging shows only one band corresponding to the molecular weight of sdAb—left lane molecular weight markers and right lane [$^{18}$F]RL-I-2Rs15d. C) Immunoreactivity assay data. D) Saturation binding assay data (Mean ± SD) obtained using BT474M1 cells.

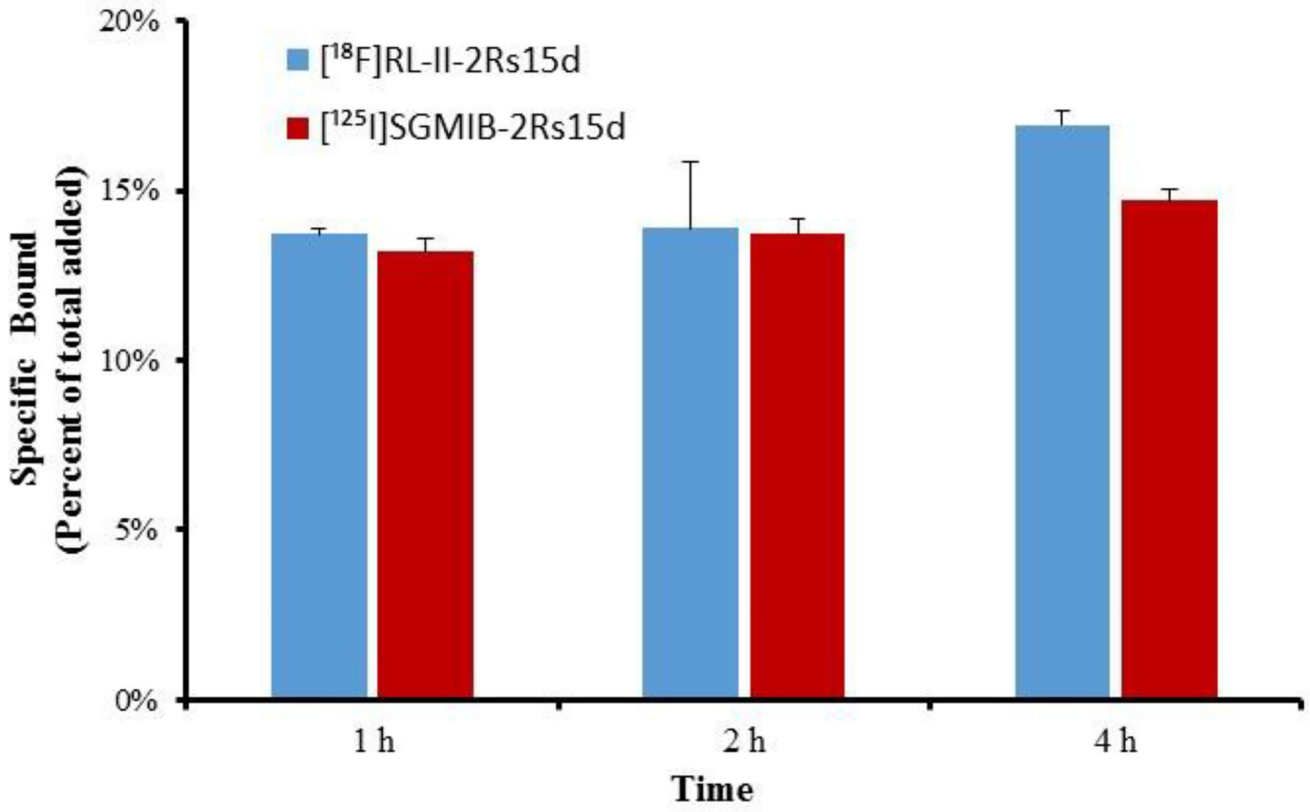


**Figure 2.**

Paired-label cellular uptake studies of [$^{125}$I]SGMIB-2Rs15d and [$^{18}$F]RL-II-2Rs15d. BT474M1 cells were incubated with[$^{125}$I]SGMIB-2Rs15d (red) and [$^{18}$F] RL-II-2Rs15d (blue) at 37 °C and processed at 1, 2, and 4 h as described in the text. Data (Mean ± SD) shown are percent of initial added radioactivity that was specifically (total minus nonspecific) cell-associated.

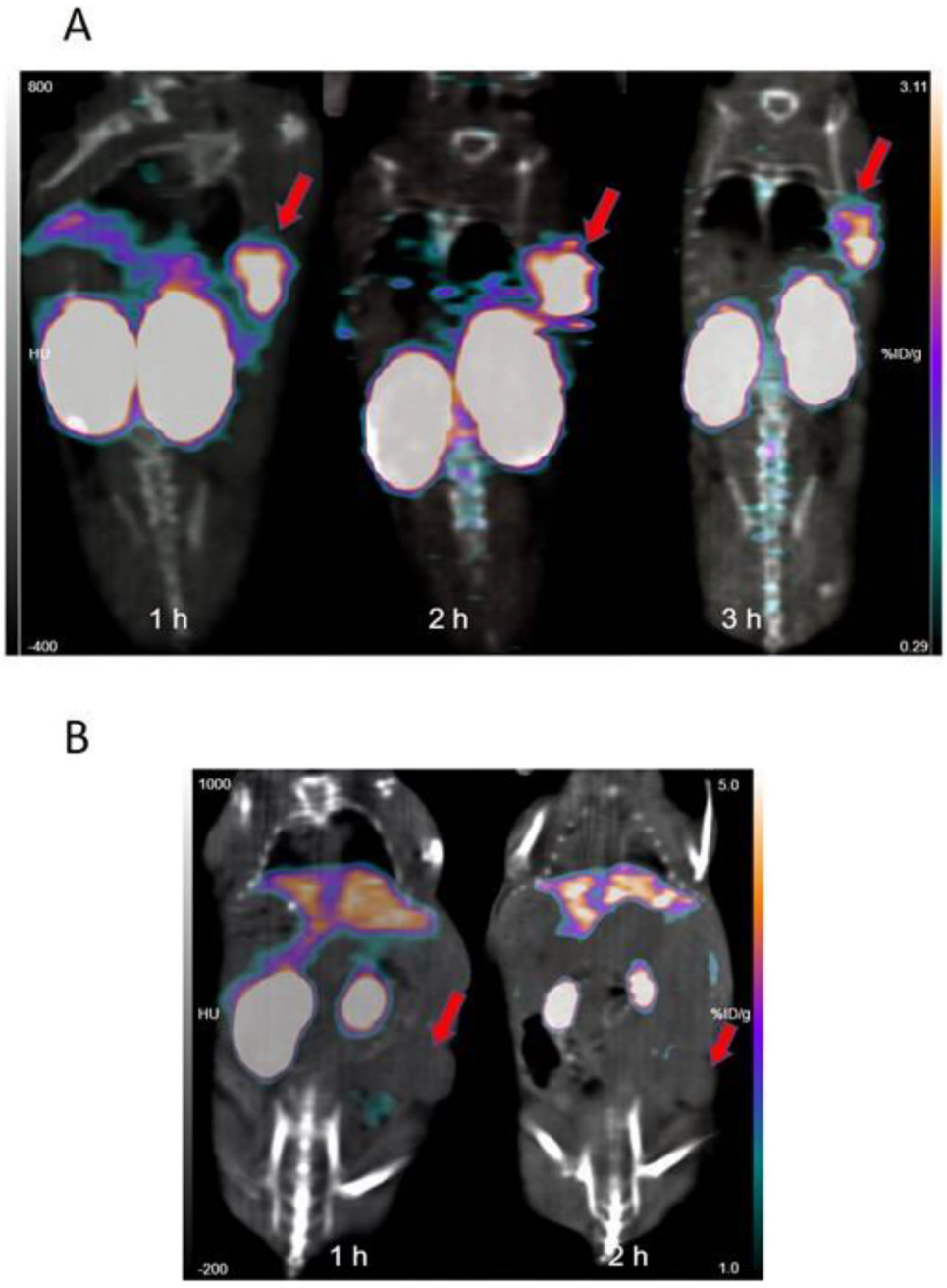


**Figure 3.**

MicroPET/CT images (coronal) obtained at 1 h, 2 h and 3 h after injection of [$^{18}$F]RL-II-2Rs15d (A) and 1 h and 2 h after injection of [$^{18}$F]RL-II-R3B23 (B) into athymic mice bearing SKOV-3 xenografts. Tumor location, which was different for the two studies, is indicated by arrows.

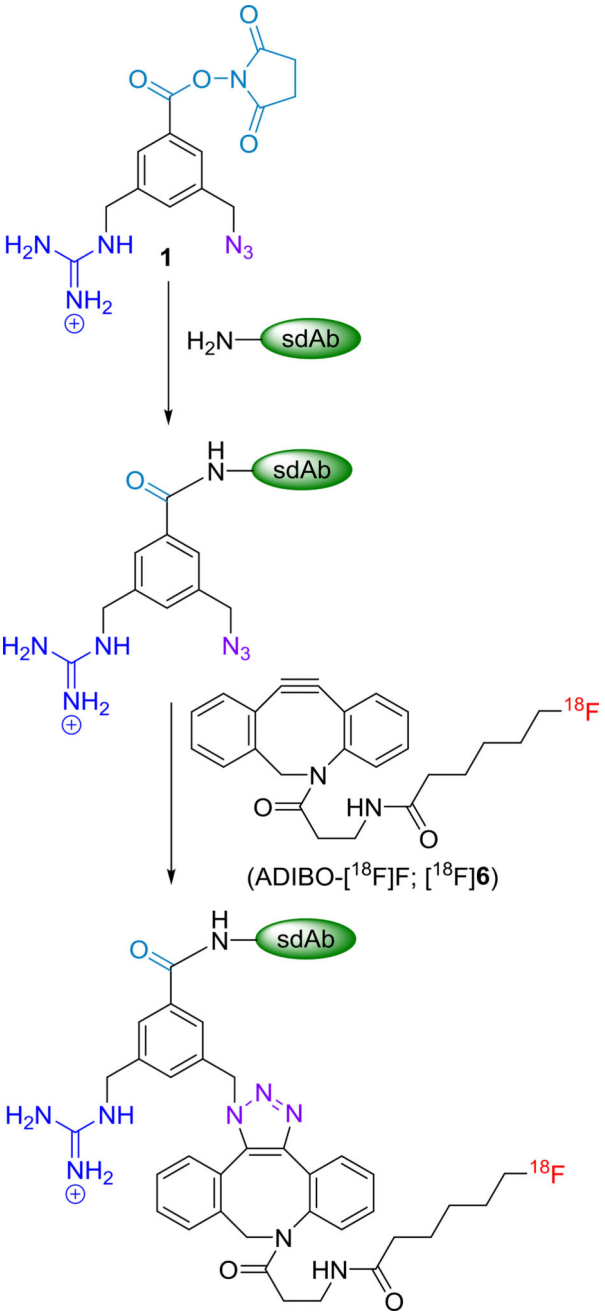


**Scheme 1.**

Pre-derivatization of sdAb with **1** and subsequent $^{18}$F-labeling via SPAAC with ADIBO-[$^{18}$F]F.

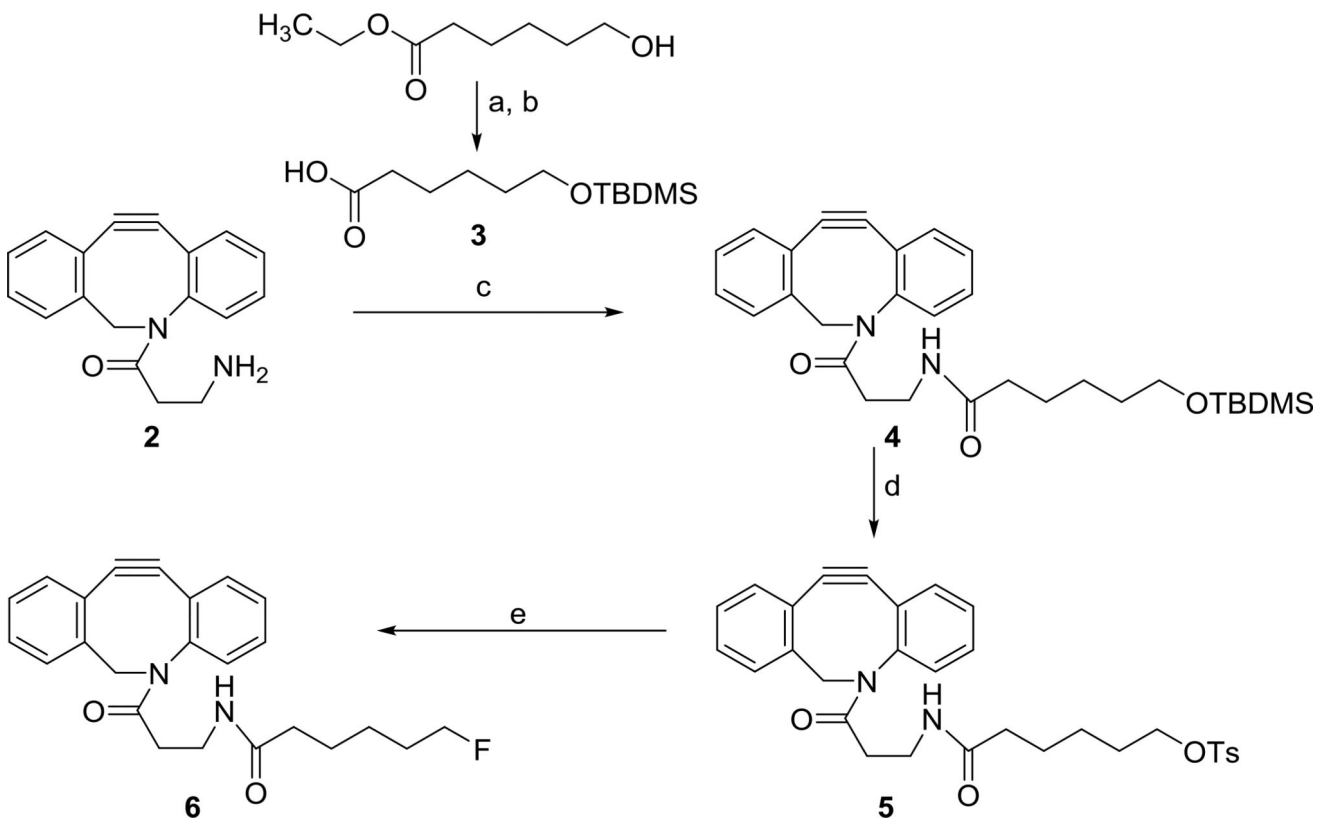


**Scheme 2.**

Scheme for the synthesis of ADIBO-OTs and ADIBO-F.

a) *tert*-butyldimethylsilyl chloride, imidazole, DMF b) TritonB, MeOH c) EDC, DMAP, *N*-hydroxysuccinimide, DMF d) TsF, DBU, MeCN e) TBAF, THF

**Table 1**

Comparison of the two methods—[$^{18}$F]RL-I and [$^{18}$F]RL-II—for $^{18}$F-labeling of 2Rs15d.

| Parameter | [$^{18}$F]RL-I | [$^{18}$F]RL-II |
|---|---|---|
| Total time for synthesis | 3 h | 2 h |
| Heating cycles | 3 | 1 |
| Total time for heating | 50 min | 15 min |
| Evaporation cycles | 6 | 4 |
| HPLC | Normal phase | Reversed-phase |
| Extraction required | Yes | No |
| Cartridge other than QMA | $Na_2SO_4$ | C18 |
| TFA cleavage required | Yes | No |
| RCY[a] for intermediate | 8.5 ± 2.8% | 55.9 ± 14.5% |
| Conjugation yield | 40.8 ± 9.1% | 23.9 ± 6.9% |
| Overall decay-corrected yield | 3.5 ± 1.0% | 3.2 ± 0.9% |

[a]RCY is radiochemical yield

## Table 2

Paired-label biodistribution of [$^{18}$F]RL-II-2Rs15d and [$^{125}$I]SGMIB-2Rs15d in athymic mice bearing subcutaneous SKOV-3 ovarian cancer xenograft.

| Tissues | Percent injected dose per gram[a] | | | |
|---|---|---|---|---|
| | 1 h | | 2 h | |
| | I-125 | F-18 | I-125 | F-18 |
| Liver | 0.36 ± 0.04 | 2.22 ± 0.56 | 0.55 ± 0.06 | 2.48 ± 0.32 |
| Spleen | 0.19 ± 0.03 | 0.78 ± 0.19 | 0.28 ± 0.06 | 0.84 ± 0.08 |
| Lungs | 0.64 ± 0.23 | 1.53 ± 0.37 | 0.45 ± 0.10 | 1.39 ± 0.43 |
| Heart | 0.23 ± 0.05 | 0.85 ± 0.23 | 0.18 ± 0.03 | 0.58 ± 0.11 |
| Kidneys | 43.37 ± 7.54 | 131.13 ± 10.73 | 24.66 ± 6.54 | 78.81 ± 11.72 |
| Stomach | 0.44 ± 0.15 | 0.69 ± 0.24[c] | 1.35 ± 0.50 | 0.54 ± 0.15 |
| Sm. Int. | 0.52 ± 0.17 | 1.49 ± 0.22 | 0.30 ± 0.06 | 1.73 ± 0.45 |
| Lg. Int. | 0.14 ± 0.03 | 0.51 ± 0.17 | 0.35 ± 0.07 | 1.45 ± 0.42 |
| Thyroid[b] | 0.04 ± 0.20 | 0.20 ± 0.11[c] | 0.70 ± 0.20 | 0.22 ± 0.06 |
| Muscle | 0.36 ± 0.30 | 0.61 ± 0.23[c] | 0.12 ± 0.06 | 0.45 ± 0.10 |
| Blood | 0.32 ± 0.12 | 0.91 ± 0.12 | 0.35 ± 0.03 | 0.62 ± 0.13 |
| Bone | 0.29 ± 0.17 | 1.38 ± 0.28 | 0.18 ± 0.04 | 2.49 ± 0.76 |
| Brain | 0.05 ± 0.03 | 0.29 ± 0.09 | 0.03 ± 0.01 | 0.30 ± 0.06 |
| Tumor | 4.80 ± 0.78 | 5.54 ± 0.77[c] | 4.78 ± 1.39 | 6.42 ± 1.70[c] |

[a] Mean ± SD (n = 5 except for bone at 1 h);

[b] Percent injected dose per organ;

[c] Difference in the uptake between the two agents statistically *not* significant.

## Table 3

Tumor-to-tissue ratios calculated for selected tissues from the biodistribution data presented in Table 1.

| | Tumor-to-tissue ratios[a] | | | |
|---|---|---|---|---|
| | 1 h | | 2 h | |
| | I-125 | F-18 | I-125 | F-18 |
| Liver | 13.53 ± 2.91 | 2.70 ± 1.07 | 8.61 ± 1.75 | 2.60 ± 0.59 |
| Spleen | 25.22 ± 6.01 | 7.57 ± 2.36 | 17.66 ± 5.05 | 7.61 ± 1.42 |
| Lungs | 8.46 ± 3.58 | 3.84 ± 1.19 | 10.64 ± 1.73 | 4.74 ± 1.06 |
| Heart | 21.32 ± 4.91 | 6.93 ± 2.10 | 26.10 ± 6.07 | 11.16 ± 2.72 |
| Kidneys | 0.11 ± 0.03 | 0.04 ± 0.01 | 0.20 ± 0.07 | 0.08 ± 0.02 |
| Muscle | 17.89 ± 8.07 | 9.92 ± 3.53[b] | 46.79 ± 23.43 | 14.81 ± 4.57 |
| Blood | 16.57 ± 6.00 | 6.23 ± 1.46 | 13.63 ± 3.54 | 10.47 ± 2.28[b] |
| Bone | 15.11 ± 9.60 | 3.61 ± 1.90 | 29.02 ± 14.66 | 2.70 ± 0.76 |

[a] Mean ± SD (n=5);

[b] Difference in ratio between the two agents statistically not significant.

**Table 4**

$^{18}$F to $^{125}$I uptake ratios obtained from the biodistribution of [$^{18}$F]RL-II-2Rs15d/[$^{125}$I]SGMIB-2Rs15d in SKOV-3 model in the current study compared with the same ratios obtained from the data for [$^{18}$F]RL-I-2Rs15d/[$^{125}$I]SGMIB-2Rs15d in BT474M1 model reported (Zhou et al., 2017).

| Tissues | $^{18}$F/$^{125}$I Ratio | | | |
|---|---|---|---|---|
| | 1 h | | 2 h | |
| | RL-I | RL-II | RL-I | RL-II |
| Liver | 10.82 ± 1.87 | 6.21 ± 1.60 | 12.15 ± 1.42 | 4.49 ± 0.26 |
| Spleen | 5.18 ± 1.46 | 4.05 ± 1.00 | 4.92 ± 0.82 | 3.11 ± 0.57 |
| Lungs | 5.02 ± 0.53 | 2.49 ± 0.55 | 4.87 ± 0.80 | 3.09 ± 0.51 |
| Heart | 2.31 ± 0.36 | 3.91 ± 1.58 | 2.12 ± 0.74 | 3.18 ± 0.46 |
| Kidneys | 1.19 ± 0.11 | 3.06 ± 0.29 | 0.88 ± 0.02 | 3.28 ± 0.43 |
| Stomach | 1.67 ± 0.27 | 1.60 ± 0.34 | 1.64 ± 0.15 | 0.42 ± 0.12 |
| Muscle | 1.39 ± 0.22 | 2.07 ± 0.76 | 1.23 ± 0.35 | 4.25 ± 1.77 |
| Blood | 1.59 ± 0.19 | 3.18 ± 1.11 | 2.07 ± 0.28 | 1.77 ± 0.30 |
| Bone | 1.83 ± 0.36 | 6.05 ± 3.33 | 2.18 ± 1.15 | 14.90 ± 6.53 |
| Brain | 1.71 ± 0.73 | 7.88 ± 5.01 | 1.22 ± 0.18 | 11.56 ± 4.57 |
| Tumor | 0.84 ± 0.03 | 1.16 ± 0.11 | 0.80 ± 0.02 | 1.35 ± 0.04 |